

# Observed dynamic performance of the Yokohama-Bay Bridge from system identification using seismic records

Dionysius M. Siringoringo and Yozo Fujino\*<sup>†</sup>

*Department of Civil Engineering, University of Tokyo, 7-3-1 Hongo, Bunkyo-ku, Tokyo 113-8656, Japan*

## SUMMARY

Strong motion data acquired from instrumented bridges during seismic events provides an excellent opportunity to gain insight into the behaviour of bridges and performance of their components. Using system identification, modal parameters of bridges can be estimated and the performance during various level of earthquake can be studied. In this study dynamic behaviour of Yokohama-Bay Bridge is investigated using seismic response recorded from six earthquakes. Modal parameters of the structure are estimated using system realization of state–space model. The realization method used here is based on the system realization using information matrix (SRIM), which makes use of the correlations between earthquake input and output data to identify the coefficient matrices of state–space model. Identification results from six earthquakes show that the system identification can be used to capture global behaviour of the bridge by estimating modal parameters and also to explain local behaviour of its component such as performance of link-bearing connections during earthquake. Copyright © 2005 John Wiley & Sons, Ltd.

KEY WORDS: system identification using seismic records; system realization using information matrix; Yokohama-Bay Bridge

## 1. INTRODUCTION

Applications of system identification for constructed civil structures are significantly important for model validation, structural assessment and monitoring. For earthquake engineering application in particular, system identification from recorded strong motion plays a vital role in gaining information concerning the seismic performance of structures and assessing the severity of earthquake effects on structures. This is especially valuable when the study of the real behaviour of systems is experimentally not feasible due to their exceptionally large inertias.

The general approach of earthquake-induced system identification is to use the input–output relation to recreate structural models that are capable of reproducing the actual responses. One

---

\*Correspondence to: Yozo Fujino, Department of Civil Engineering, University of Tokyo, 7-3-1 Hongo, Bunkyo-ku, Tokyo 113-8656, Japan.

<sup>†</sup>E-mail: fujino@civil.t.u-tokyo.ac.jp

Contract/grant sponsor: Japanese Ministry of Education, Culture, Sports, Science and Technology

of the early studies on this was made by Beck and Jennings [1] that uses the output-error minimization method for linear, time-invariant structural systems with classical damping. In the same approach, but using frequency domain McVerry [2] utilizes a transfer function to minimize the objective function of output error. Chaudhary *et al.* [3] improves it for a more general problem of non-classical damping which includes the structural model in addition to the modal model. The last method, while powerful and significantly insightful into the structural model, requires prior information of structural properties that are typically unavailable and difficult to obtain, especially for large and complex structures. Most approaches are developed in the frequency domain, which is mainly due to the tradition of experienced personnel and vast application of instrument for measurement. These approaches offer advantages in incorporating soil–structure interaction into analysis, but suffer when closely spaced modes are present or high frequency resolution and non-linear identification is required [4]. Other considerable effort and discussion on system identification of civil structures can be found in the works by Masry [5, 6], Udawadia [7], Safak [8, 9] and Beck and Katafygiotis [10, 11].

Recent advances in the study of state–space models for modal parameter identification have led to the development of a new technique in time domain. This technique makes use of an input–output mapping technique to determine the impulse response histories which is also known as Markov parameter of linear system. The methodology, referred to as observer/Kalman filter identification algorithm (OKID) [12], is formulated entirely in the time-domain and does not require any prior knowledge of structural properties. This algorithm has shown its high capability in identifying structural modal parameters when it is used in conjunction with eigensystem realization algorithm (ERA) [13] or eigensystem realization algorithm with data correlation method (ERA/DC) [14]. The ERA/DC uses the shifted data correlation of the pulse response and factors the correlation matrix via singular value decomposition to realize system matrices. The OKID-ERA algorithm is capable of handling general multi-input multi-output response even with high-frequency resolution and is especially promising for control and earthquake engineering problem. Using a similar approach, Juang [15] developed the system realization using information matrix (SRIM). In this algorithm, system identification is performed directly from input and output data without the need to obtain pulse response or Markov parameters using the observer/Kalman filter identification (OKID) technique. This eases the computational burden in identification and thus SRIM can be considered an improvement over and extension of ERA/DC.

The increasing number of instrumented bridges, especially the long span ones has made the application of system identification for structural assessment significantly important. Moreover, due to limited earthquake records available from such bridges, their actual performance during earthquakes remains to be thoroughly investigated. Recently, Smyth *et al.* [16] performed system identification of the Vincent Thomas Suspension Bridge subjected to the 1987 Whitter Narrows and the 1994 Northridge earthquakes. In that study, the methodology was based on the least-square solution of a reduced-order of discrete dynamic system. This approach, while simple and powerful in identifying the non-linearity, requires the measurement of displacement and velocity in addition to acceleration, which are typically not available and must be integrated from the acceleration time-histories. Generally this causes problem with accuracy especially in the case where acceleration records contain noise in the low frequencies. Lus and Betti [17] have reported the successful application of OKID-ERA for the identification of the same bridge. The results of identification show that the impulse response histories obtained from the input–output

mapping technique can be used to determine the state–space models of a large and complex 3-D MIMO structural system.

In this paper the application of the SRIM-based approach for the identification of dynamic characteristics of Yokohama-Bay Bridge subjected to seismic excitation is presented. The research described in this paper involves:

- (1) Identification of dynamic characteristics of Yokohama-Bay Bridge from seismic records. This includes comparison of the identification from seismic records with an analytical finite element model, previous test using ambient vibration, and forced vibration.
- (2) Study of the effect of ground motion intensity with respect to the results of system identification. Two cases are evaluated namely the global behaviour of modal parameters and observation of link-bearing performance during various ground motion.

## 2. DESCRIPTION OF YOKOHAMA-BAY BRIDGE

The bridge investigated in this research is Yokohama-Bay Bridge, located at the entrance of Yokohama harbour and is a vital part of the Yokohama-Tokyo bay-shore expressway (see Figure 1). It is a continuous three-span cable-stayed bridge with the main girder consisting of a double-deck steel truss-box. The central span is 460 m with side spans of 200 m each. The upper and lower deck have 6 and 2 lanes, respectively, with the upper deck being part of the Yokohama Expressway Bay shore Route and the lower deck a part of the National Route. The bridge has two H-shaped towers of 172 m height and 29.25 m width with a welded monolithic section. Earthquake resistance of the bridge was carefully reviewed in design. Considering the possibility of a large event like the Great Kanto earthquake that Tokyo and Yokohama experienced in 1923, the weak ground and higher centre of gravity of bridge, the girder is suspended from the towers and end-piers with link bearing in such a way that the effect of the superstructure on the substructure during an earthquake is reduced by maintaining a long fundamental period about 7.7 s in the longitudinal direction. The structure, with its long natural period, is expected to see lower acceleration during an earthquake but, on the other hand, its displacement is increased. Therefore to restrict the horizontal displacement during earthquake, short links with the length of 2 m and shape of inverted pendulum were utilized to connect the girder with the towers and end piers.

Many large bridges including Yokohama-Bay Bridge were designed and constructed before the 1995 Hyogo-ken Nanbu (Kobe) Earthquake. The near-field ground motions measured during the 1995 Kobe Earthquake were extremely severe and much larger than what was specified in the bridge design codes at that time. Seismic retrofit program of bridges has also started in Japan after the Kobe earthquake and the bridge seismic design code was later revised to anticipate the similar ground motions experienced in Kobe. In Reference [18] Fujino *et al.* presents a thorough reviewed design for seismic capacity of the Yokohama-Bay Bridge. Fortunately, the bridge is heavily instrumented and analysing the records from the past seismic events allow us to capture the real performance of the bridge under seismic excitations, which is extremely important in seismic retrofit design.



Figure 1. Yokohama-Bay Bridge.

### 3. SYSTEM IDENTIFICATION METHODOLOGY

#### 3.1. Basic formulation

The equation of motion for an  $N$  degree-of-freedom (DOF) linear, time invariant, viscously damped system subjected to earthquake excitation  $\alpha(t)$ , in the spatial coordinate  $\mathbf{u}(t)$  and continuous time is given as

$$\mathbf{M}\ddot{\mathbf{u}}(t) + \mathbf{C}\dot{\mathbf{u}}(t) + \mathbf{K}\mathbf{u}(t) = -\mathbf{W}\alpha(t) \quad (1)$$

where  $\mathbf{M}$ ,  $\mathbf{C}$  and  $\mathbf{K} \in \mathbb{R}^{N \times N}$  are mass, damping and stiffness matrices, respectively, while the  $\mathbf{W} \in \mathbb{R}^{N \times q}$  is the continuous time input matrix, with  $q$  being the dimension of input vector  $\alpha(t)$ . This equation can be expressed in a finite dimensional, discrete-time, linear, time-invariant, state variable dynamical system as

$$\mathbf{x}(k+1) = \mathbf{A}\mathbf{x}(k) + \mathbf{B}\mathbf{z}(k) \quad (2a)$$

$$\mathbf{y}(k) = \mathbf{R}\mathbf{x}(k) + \mathbf{D}\mathbf{z}(k) \quad (2b)$$

The vector  $\mathbf{x}(k) = [u(k) \ \dot{u}(k)]^T$  in the later expression is a  $2N \times 1$  state vector consisting of displacement and velocity. Vector  $\mathbf{z}(k)$  denotes the  $q \times 1$  input acceleration of ground motion and  $\mathbf{y}(k)$  denotes the  $m \times 1$ , structural acceleration responses as outputs. The integer  $k = 0, 1, 2, \dots, l$  denotes the time-step number, i.e.  $\mathbf{x}(k+1) = \mathbf{x}(k(\Delta t) + \Delta t)$ , with  $\Delta t$  being the time interval. The quantities of  $\mathbf{A} \in \mathbb{R}^{2N \times 2N}$ ,  $\mathbf{B} \in \mathbb{R}^{2N \times q}$ ,  $\mathbf{R} \in \mathbb{R}^{m \times 2N}$  and  $\mathbf{D} \in \mathbb{R}^{m \times q}$  are the discrete representation of system matrices. Their corresponding continuous system matrices

are given as

$$\begin{aligned} \mathbf{A} &= e^{\mathbf{A}_c \Delta t}, \quad \mathbf{B} = \left[ \int_0^{\Delta t} e^{[\mathbf{A}_c] \tau'} d\tau' \mathbf{B}_c \right] \\ \mathbf{R} &= \mathbf{L}[-\mathbf{M}^{-1} \mathbf{K} \quad -\mathbf{M}^{-1} \mathbf{C}], \quad \mathbf{D} = \mathbf{L} \mathbf{M}^{-1} \end{aligned} \quad (3)$$

Matrix  $[\mathbf{L}] \in \mathbb{R}^{m \times N}$  is a transformation matrix that connects the position of system degree-of-freedom with the measured structural output responses. Matrix  $\mathbf{A}_c \in \mathbb{R}^{2N \times 2N}$  is a system matrix in continuous time and  $\mathbf{B}_c \in \mathbb{R}^{2N \times q}$  is the input influence matrix of order  $2N \times q$ , defined as follows:

$$\mathbf{A}_c = \begin{bmatrix} \mathbf{0} & \mathbf{I} \\ -\mathbf{M}^{-1} \mathbf{K} & -\mathbf{M}^{-1} \mathbf{C} \end{bmatrix}, \quad \mathbf{B}_c = \begin{bmatrix} \mathbf{0} \\ -\mathbf{I} \end{bmatrix} \quad (4)$$

The time discretization error that might appear may be made negligible by using a sufficiently small time step. Since most earthquake excitation is sampled at the frequency of 100 Hz, which is sufficiently small as compared to the most natural frequencies of civil structures (i.e. far below 50 Hz), discretization error in this case might be negligible. The system matrices  $\mathbf{A} \in \mathbb{R}^{2N \times 2N}$ ,  $\mathbf{B} \in \mathbb{R}^{2N \times q}$ ,  $\mathbf{R} \in \mathbb{R}^{m \times 2N}$  and  $\mathbf{D} \in \mathbb{R}^{m \times q}$  are unknowns and are to be determined from given input-output earthquake data. With several algebraic manipulations, Equation (2) can be rewritten for various  $p$  time spans in a matrix form as

$$\mathbf{y}_p(k) = [\mathbf{O}_p] \mathbf{x}(k) + [\mathbf{T}_p] \mathbf{z}_p(k) \quad (5)$$

where the  $\mathbf{y}_p(k)$ ,  $\mathbf{z}_p(k)$ ,  $[\mathbf{O}_p]$  and  $[\mathbf{T}_p]$  are defined as follows:

$$\begin{aligned} \mathbf{y}_p(k) &= \begin{bmatrix} y(k) \\ y(k+1) \\ y(k+2) \\ \vdots \\ y(k+p-1) \end{bmatrix} \quad [\mathbf{O}_p] = \begin{bmatrix} \mathbf{R} \\ \mathbf{R}\mathbf{A} \\ \mathbf{R}\mathbf{A}^2 \\ \vdots \\ \mathbf{R}\mathbf{A}^{p-1} \end{bmatrix} \quad \mathbf{z}_p(k) = \begin{bmatrix} z(k) \\ z(k+1) \\ z(k+2) \\ \vdots \\ z(k+p-1) \end{bmatrix} \\ [\mathbf{T}_p] &= \begin{bmatrix} \mathbf{D} & & & & \\ \mathbf{R}\mathbf{B} & \mathbf{D} & & & \\ \mathbf{R}\mathbf{A}\mathbf{B} & \mathbf{R}\mathbf{B} & \mathbf{D} & & \\ \vdots & \vdots & \dots & \ddots & \\ \mathbf{R}\mathbf{A}^{p-2}\mathbf{B} & \mathbf{R}\mathbf{A}^{p-3}\mathbf{B} & \mathbf{R}\mathbf{A}^{p-4}\mathbf{B} & \dots & \mathbf{D} \end{bmatrix} \end{aligned} \quad (6)$$

The matrix  $[\mathbf{O}_p] \in \mathbb{R}^{pm \times 2N}$  is commonly called the observability matrix. The matrix  $[\mathbf{T}_p] \in \mathbb{R}^{pm \times pq}$  is a generalized Toeplitz matrix composed of the system Markov parameters (i.e.  $\mathbf{R}\mathbf{A}^{k-1}\mathbf{B}$ ) and is therefore unique even though the system matrices  $\mathbf{A}$ ,  $\mathbf{B}$ ,  $\mathbf{R}$  and  $\mathbf{D}$  are not unique.

### 3.2. System realization using information matrix

The SRIM algorithm starts by identifying the observability matrix  $[\mathbf{O}_p]$ . Let  $[\mathbf{O}_p](m+1 : pm, :)$  be defined as the matrix consisting of the last  $(p-1)m$  rows (from the  $(m+1)$ th row until the  $(pm)$ th row) and all columns of  $[\mathbf{O}_p]$ . Similarly the  $[\mathbf{O}_p](1 : (p-1)m, :)$  is defined as a matrix consists of the first  $(p-1)m$  rows and all columns of  $[\mathbf{O}_p]$ . The above definitions are rewritten in matrix form as follows:

$$[\mathbf{O}_p](m+1 : pm, :) = \begin{bmatrix} \mathbf{R}\mathbf{A} \\ \mathbf{R}\mathbf{A}^2 \\ \mathbf{R}\mathbf{A}^3 \\ \vdots \\ \mathbf{R}\mathbf{A}^{p-1} \end{bmatrix} \quad \text{and} \quad [\mathbf{O}_p](1 : (p-1)m, :) = \begin{bmatrix} \mathbf{R} \\ \mathbf{R}\mathbf{A} \\ \mathbf{R}\mathbf{A}^2 \\ \vdots \\ \mathbf{R}\mathbf{A}^{p-2} \end{bmatrix} \quad (7)$$

Now, following the equality

$$[\mathbf{O}_p](m+1 : pm, :) = \begin{bmatrix} \mathbf{R}\mathbf{A} \\ \mathbf{R}\mathbf{A}^2 \\ \mathbf{R}\mathbf{A}^3 \\ \vdots \\ \mathbf{R}\mathbf{A}^{p-1} \end{bmatrix} = \begin{bmatrix} \mathbf{R} \\ \mathbf{R}\mathbf{A} \\ \mathbf{R}\mathbf{A}^2 \\ \vdots \\ \mathbf{R}\mathbf{A}^{p-2} \end{bmatrix} \mathbf{A} = [\mathbf{O}_p](1 : (p-1)m, :)\mathbf{A} \quad (8)$$

the state matrix  $[\mathbf{A}]$  can be identified as

$$[\mathbf{A}] = [\mathbf{O}_p^*](1 : (p-1)m, :)[\mathbf{O}_p](m+1 : pm, :) \quad (9)$$

where the asterisk (\*) denotes the pseudo inverse matrix. Following the derivation in Equations (6) and (7), the choice of integer  $p$  becomes obvious. The integer  $p$  should be chosen such that matrix  $[\mathbf{O}_p](m+1 : pm, :)$  of dimension  $(p-1)m \times 2N$  has rank larger than or equal to  $2N$ , hence  $p \geq (2N/m) + 1$ .

Following the derivation above, it is obvious that to obtain system realization, one needs to estimate the observability matrix  $[\mathbf{O}_p]$  from the given input–output data. To obtain the observability matrix, the procedure is started by expanding the vector Equation in (5), to a matrix equation, i.e.

$$[\mathbf{Y}_p](k) = [\mathbf{O}_p]\mathbf{X}(k) + [\mathbf{T}_p][\mathbf{Z}_p](k) \quad (10)$$

where

$$\mathbf{X}(k) = [x(k) \quad x(k + 1) \quad \cdots \quad x(k + s - 1)]$$

$$\begin{aligned} [\mathbf{Y}_p] &= [y_p(k) \quad y_p(k + 1) \quad \cdots \quad y_p(k + s - 1)] \\ &= \begin{bmatrix} y(k) & y(k + 1) & \cdots & y(k + s - 1) \\ y(k + 1) & y(k + 2) & \cdots & y(k + s) \\ \vdots & \vdots & \ddots & \vdots \\ y(k + p - 1) & y(k + p) & \cdots & y(k + p + s - 2) \end{bmatrix} \\ [\mathbf{Z}_p] &= [z_p(k) \quad z_p(k + 1) \quad \cdots \quad z_p(k + s - 1)] \\ &= \begin{bmatrix} z(k) & z(k + 1) & \cdots & z(k + s - 1) \\ z(k + 1) & z(k + 2) & \cdots & z(k + s) \\ \vdots & \vdots & \ddots & \vdots \\ z(k + p - 1) & z(k + p) & \cdots & z(k + p + s - 2) \end{bmatrix} \end{aligned} \tag{11}$$

To ensure that the rank of  $[\mathbf{Y}_p]$  and  $[\mathbf{Z}_p]$  is at least equal to that of matrix  $[\mathbf{O}_p]$  the integer  $s$  must be selected to be sufficiently large. Thus, rank evaluation must be performed before selecting the proper value for integer  $s$ . Now let us define the following quantities:  $\mathbf{R}_{yy}$ ,  $\mathbf{R}_{zz}$ ,  $\mathbf{R}_{xx}$ ,  $\mathbf{R}_{yz}$ ,  $\mathbf{R}_{yx}$ , and  $\mathbf{R}_{xz}$  as correlation matrix between input ( $z$ ), output ( $y$ ), and state ( $x$ ), respectively, where the subscript indices denote the product of correlation in such a way that the correlation of  $\mathbf{A}_p$  and  $\mathbf{B}_p$  is defined as

$$\mathbf{R}_{ab} = \frac{1}{s} \mathbf{A}_p(k) \mathbf{B}_p^T(k) \tag{12}$$

If the integer  $s = l - p$  is sufficiently large, with  $l$  being the total data length and  $p$  the data shift, the quantities in Equation (10) approximate the expected values in a statistical sense. To determine the observability matrix  $[\mathbf{O}_p]$ , one can start by obtaining the data correlations of input–output matrices

$$\mathbf{R}_{hh} = [\mathbf{O}_p] \hat{\mathbf{R}}_{xx} [\mathbf{O}_p]^T \tag{13}$$

where the quantities  $\mathbf{R}_{hh}$  and  $\hat{\mathbf{R}}_{xx}$  are defined as follows:

$$\mathbf{R}_{hh} = \mathbf{R}_{yy} - \mathbf{R}_{yz} \mathbf{R}_{zz}^{-1} \mathbf{R}_{yz}^T \tag{14a}$$

$$\hat{\mathbf{R}}_{xx} = \mathbf{R}_{xx} - \mathbf{R}_{xz} \mathbf{R}_{zz}^{-1} \mathbf{R}_{xz}^T \tag{14b}$$

The quantity  $\mathbf{R}_{hh}$  is determined from the output autocorrelation matrix  $\mathbf{R}_{yy}$ , the input–output cross-correlation matrix  $\mathbf{R}_{yz}$  and the inverse of input autocorrelation matrix, which are all available from input–output data. Note that the quantity of  $\mathbf{R}_{hh}$  exists only if the input autocorrelation matrix  $\mathbf{R}_{zz}$  is a non-singular matrix. This requirement will be satisfied if the

input is persistent and rich enough for  $z(k)$ , with  $k = 0, 1, \dots, l$  or in other words the input block matrix  $\mathbf{Z}_p(\mathbf{k})$  is of full rank (i.e.  $qp$ ). If we assume that the input and the state vectors are two uncorrelated quantities, then the cross-correlation matrix between them  $\mathbf{R}_{xz}$  becomes a  $2N \times qp$  zero matrix, and Equation (14b) thus reduces to  $\hat{\mathbf{R}}_{xx} = \mathbf{R}_{xx}$ . This condition can be achieved if the input is a sufficiently long Gaussian random signal. With this assumption, Equation (13) can be solved for matrix  $[\mathbf{O}_p]$ , given the matrix  $\mathbf{R}_{hh}$  computed from input–output data. To obtain the solution for matrix  $[\mathbf{O}_p]$ , Equation (13) needs to be factored into three matrices where the first matrix is the transpose product of the third matrix. The singular value decomposition is a logical choice for this matrix factorization. In this decomposition, only the first size  $(pm \times (p-1)m)$  row and column of  $\mathbf{R}_{hh}$  matrix is decomposed using singular value decomposition. The new form of decomposition is

$$\mathbf{R}_{hh}(:, 1 : (p-1)m) = \mathbf{H}\Sigma^2\mathbf{V}^T = \begin{bmatrix} \bar{\mathbf{H}}_{2N} & \bar{\mathbf{H}}_0 \end{bmatrix} \begin{bmatrix} \Sigma_{2N}^2 & 0_{2N \times n_0} \\ 0_{m_0 \times 2N} & 0_{m_0 \times n_0} \end{bmatrix} \begin{bmatrix} \mathbf{V}_{2N}^T \\ \mathbf{V}_0^T \end{bmatrix} = \mathbf{V}_{2N}\Sigma_{2N}^2\mathbf{V}_{2N}^T \quad (15)$$

where the dimension of  $\mathbf{R}_{hh}(:, 1 : (p-1)m)$  is  $(pm \times (p-1)m)$ . The integer  $n_0$  indicates the number of zero singular values and also the number of columns of  $\mathbf{V}_0$ . The integer  $m_0$  denotes the numbers of columns in  $\bar{\mathbf{H}}_0$  that are orthogonal to the column in  $\bar{\mathbf{H}}_{2N}$ . For noisy data, there are no zero singular values, that is,  $n_0 = 0$ . If no singular values are truncated,  $m_0 = m$  is obtained. If some singular values are truncated,  $m_0$  becomes the sum of  $m$ . Whichever the condition of singular values truncation is, the partial decomposition method guaranties that there are at least  $m$  columns of  $\bar{\mathbf{H}}_0$  that are orthogonal to the columns of  $\bar{\mathbf{H}}_{2N}$  in Equation (15). Further factorization of Equation (13) produces

$$\mathbf{R}_{hh}[:, 1 : (p-1)m] = [\mathbf{O}_p]\hat{\mathbf{R}}_{xx}[\mathbf{O}_p]^T[:, 1 : (p-1)m] = \bar{\mathbf{H}}_{2N}\Sigma_{2N}^2\mathbf{V}_{2N}^T \quad (16)$$

Finally following the identity in Equation (16), the observability matrix can be obtained

$$[\mathbf{O}_p] = \bar{\mathbf{H}}_{2N} \quad \text{and} \quad \hat{\mathbf{R}}_{xx}[\mathbf{O}_p]^T[:, 1 : (p-1)m] = \Sigma_{2N}^2\mathbf{V}_{2N}^T \quad (17)$$

Given the observability matrix, the system matrix  $\mathbf{A}$  can be estimated from Equation (9).

### 3.3. Identification of modal parameters

Modal parameters of structural system can be estimated by solving the eigenvalue problem of matrix  $\mathbf{A}$  as follows:

$$\mathbf{A}\hat{\Phi} = \tilde{\Lambda}\hat{\Phi} \quad (18)$$

Matrices  $\tilde{\Lambda}$  and  $\hat{\Phi}$  denote the eigenvalues and eigenvectors of matrix  $\mathbf{A}$ , respectively. The eigenvalues and eigenvectors can be real or complex, where in the latter case, they appear in complex conjugate pairs. The eigenvalues  $\tilde{\lambda}_i$  are actually expressed in  $z$ -domain, and therefore, can be related to the modal characteristics of dynamic system using the following transformation:

$$\lambda_i = \frac{\ln(\tilde{\lambda}_i)}{\Delta t} \quad (19)$$

After transformation, the natural frequency ( $\omega_i$ ) and modal damping ratio ( $\xi_i$ ) can be estimated as

$$\omega_i = \sqrt{\text{Re}(\lambda_i)^2 + \text{Im}(\lambda_i)^2}, \quad \xi_i = \frac{-\text{Re}(\lambda_i)}{\omega_i} \quad (20)$$

The matrix of mode shapes in co-ordinate system is obtained by transforming the eigenvectors in  $z$ -domain into co-ordinate-domain using the output-transformation matrix  $\mathbf{R}$

$$\Phi = \mathbf{R}\hat{\Phi} \quad (21)$$

A numerical simulation using a three-dimensional (3-D) model of cable-stayed bridge for Finite Element program is performed to examine the applicability of the SRIM method [19]. Results show that under reasonable number of output sensor, modal parameters of the bridge subjected to simulated filtered-short ground motion can be estimated with a great accuracy. Using 21 sensors, 42 low order modes in three directions can be identified with high accuracy. The errors of natural frequencies estimates were found less than 2%, while the error of damping estimates reach the maximum of 15%.

## 4. APPLICATION

### 4.1. Instrumentation and sensor arrangement

As part of a monitoring system, the Yokohama-Bay bridge is equipped with 85 channels of embedded sensors measuring acceleration responses at 36 locations in three directions. These accelerometers have a range of frequency between 0.05 and 35 Hz with an accuracy of 15  $\mu\text{A}/\text{gal}$ . Among these 85 channels, 25 are located on the substructure (such as pile foundation and pile caps) and the rest are installed on the superstructure (towers, pier caps and girder). Along the girder, sensors were installed at 9 locations with a space of 115 m between each. These sensors measure accelerations vertically, laterally (out-of-plane) and longitudinally (bridge axis). On one side of the bridge girder, starting from the Honmoku approach until the middle of the main span, accelerometers were installed only along one longitudinal axis of the bridge. On the other side, starting from the middle of the main span to the Daikoku approach, accelerometers were installed on both sides of the girder, thus providing adequate information for identification of torsional modes. Both towers are equipped with accelerometers measuring longitudinal and lateral movement at both of the bridge's H-shaped towers. This enables the identification of pure longitudinal, lateral and torsional modes. For end-piers, accelerometers were installed on the pile cap and pier cap. Using the response from the sensors on the pier cap and the girder just above the pier cap, one can observe the behaviour of link-bearings connecting the girder with the towers and with the end-piers. Figure 2 illustrates sensor positioning and measuring direction.

### 4.2. Input-output data sets and description of seismic record

Three sets of input-output data are studied to represent three types of bridge motion, namely longitudinal-longitudinal motion, longitudinal-vertical motion and longitudinal-lateral motion. For the first input-output data set, responses were obtained from 20 output sensors: 4 sensors along one side of the girder, 10 sensors at both towers and 6 sensors at both piers

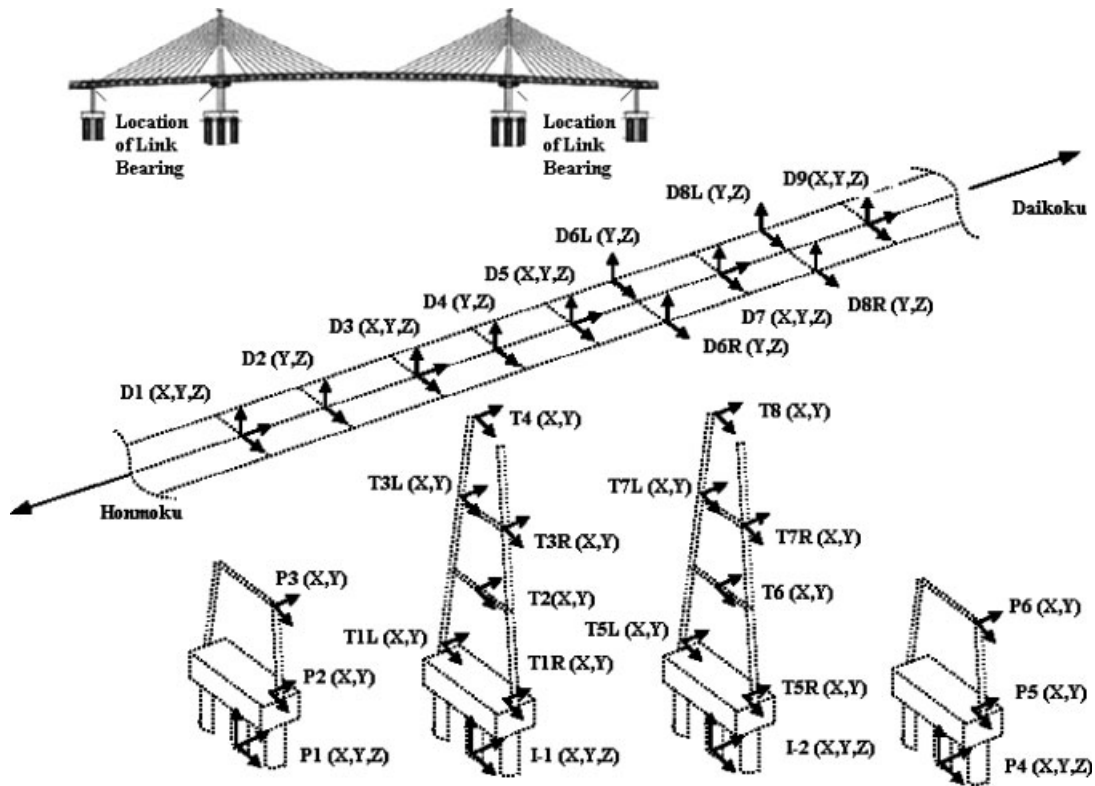


Figure 2. Bridge layout and sensor position.

Table I. Sensor arrangement for system identification of Yokohama-Bay Bridge.

System	Output sensors	
Longitudinal-longitudinal	$D1-X, D3-X, D5-X, D7-X, T5R-X, T5L-X, T7R-X, T7L-X, T8-X$	$T1R-X, T1L-X, T3L-X, T3R-X, T4-X, P1-X, P2-X, P3-X, P4-X, P5-X, P6-X$
Vertical-longitudinal	$D1-Z, D2-Z, D3-Z, D4-Z, D5-Z, D6L-Z, T1-XR, T2-X, T3R-X, T4-X$	$D6R-Z, D7-Z, D8R-Z, D8L-Z, D9-Z, T5R-X, T6-X, T7R-X, T8-X$
Lateral-longitudinal	$D1-Y, D2-Y, D3-Y, D4-Y, D5-Y, D6-YL, T1-YR, T1-YL, T3-YL, T3-YR, T4-Y$	$D7-Y, D8L-Y, D9-Y, T5-YR, T5-YL, T7-YR, T7-YL, T8-Y$

(all are measuring accelerations in the longitudinal direction). In the second input-output data set, output responses are from 11 girder sensors in the vertical ( $z$ ) direction and 8 tower sensors in the longitudinal ( $x$ ) direction. Lastly, for the third set, outputs consist of acceleration responses from 9 girder sensors and 10 tower sensors, all measuring motion in the lateral ( $y$ ) direction. Details of sensor configuration for the three sets are given in Table I. For the first

analysis, record from the 20 February 1990 Oshima Island earthquake is utilized (i.e. earthquake number 9 in Table III). The total record length is 195.5 s, this record was divided into three frames of data, where each frame consists of 6000 data points. System identification is performed using the first frame, where the peak acceleration ( $12.04 \text{ cm/s}^2$ ) resides.

## 5. RESULTS OF SYSTEM IDENTIFICATION

A total of fifteen lower modes were identified from analysis, the first swing mode in the longitudinal direction, eight modes in the vertical direction, and six modes in the lateral direction. In the first input–output data set (i.e. longitudinal direction) the first longitudinal mode was identified at 0.128 Hz, which is a typical first mode when compared to the finite element model. This mode shows a relatively large modal displacement between the end-pier's cap and the girder, indicating a hinge mechanism between the pier-cap and girder during the earthquake. In the vertical set, five bending modes and three torsion modes were identified. Their natural frequencies were found to be in good agreement with the results from the previous test and the finite element model. It should be noted that several modes that were not identified during the forced vibration and ambient test were identified from earthquake records. These are the higher vertical modes: second symmetric bending mode, third asymmetric bending mode and also two torsional modes.

In the lateral direction, six modes were identified. The first three modes were found to be closely spaced in frequency, and the main differences are the modal displacement of both towers. The first two modes are symmetric, the main difference being the phase between the towers and the girder. In the first mode, both towers were in phase with each other, and with the lateral girder. In the second mode both towers were in phase with each other, but out of phase with the lateral displacement of girder. The anti-phase of towers was observed in the third mode and the fourth mode while the lateral girder were asymmetric. List of the identified mode is shown in Table II and examples of the shapes are depicted in Figure 3.

The identification results are also compared with the results from the Finite Element Model, ambient vibration test and the forced vibration test [20], which were performed immediately after construction was completed. Identified natural frequencies are found to be in good agreement with the values previously identified from the ambient vibration test, forced vibration test, and are within a reasonable range from the FEM results. Damping ratios are identified with average values within the range of 1.0–5.2%; the highest damping occurred in the longitudinal sway mode. Most damping ratios of vertical modes are identified with the range of 1–3%, while the lateral modes are found slightly higher (1.0–4.5%). These values are higher than previously estimated (around 2%) from ambient and forced vibration tests.

## 6. OBSERVATION OF MODAL PARAMETERS FORM SEVERAL SEISMIC RECORDS

For the second analysis, seismic records with varying amplitude obtained from six major earthquakes from 1990 to 1997 were utilized. These acceleration records were divided into ten frames. The strongest ground motion was recorded during 2 February 1992 (Earthquake No. 10), with a peak acceleration of  $13.1 \text{ cm/s}^2$ . A list of the earthquakes and their intensities are shown in Table III. Modal parameters for these ten records were calculated separately.

Table II. Identified modes, natural frequencies and damping ratios of Yokohama-Bay Bridge from the February 20 1990, earthquake (frame no. 1).

Mode Description	Identified		FEM [20]	Ambient test [20]	Forced vibration [20]
	Freq (Hz)	Damp (%)			
Longitudinal					
1st Swing Mode	0.13	5.20	0.14	—	—
Vertical					
1st Symmetric Bending	0.36	3.91	0.34	0.36	0.34–0.35
1st Asymmetric Bending	0.55	3.76	0.49	0.60	0.54–0.57
2nd Symmetric Bending	0.81	1.36	0.77	0.85	0.80
2nd Asymmetric Bending	1.01	1.11	1.22	1.01	—
3rd Symmetric Bending	1.21	1.04	N/A	N/A	—
1st Torsional	0.86	1.93	0.95	0.88	—
2nd Torsional	1.38	2.10	N/A	N/A	—
3rd Torsional	2.46	1.55	N/A	N/A	—
Lateral					
1st Symmetric Bending	0.30	4.29	0.28	0.27	—
Tower-Girder same phase					
1st Symmetric Bending	0.42	4.64	N/A	N/A	—
Tower-Girder anti phase					
1st Asymmetric Bending	0.39	1.55	0.42	0.38	—
Tower anti phase					
1st Asymmetric Bending	0.75	2.27	0.70	0.68	—
Tower-Girder anti phase					
1st Asymmetric Bending	0.94	3.84	N/A	N/A	—
Tower same phase					
2nd Symmetric Bending	1.06	3.20	1.08	—	—

### 6.1. Amplitude dependency of modal parameters

Identified modal frequencies and damping ratios are plotted as functions of the root-mean-square (RMS) of the band-pass filtered input acceleration for a particular range of frequency of interest, which is the frequency range where each mode is found. For this purpose the Butterworth filter is used. This procedure is employed to ensure that only input responses within the frequency range of interest were considered in the comparison. Figures 4 and 5 show the results from comparing the natural frequencies and damping ratios of vertical and lateral modes with respect to earthquake input amplitude. The following trends are observed from the results:

- (1) Natural frequencies for bending modes in vertical and lateral directions, as well as the torsional modes are generally constant without significant changes with respect to the input amplitude. Some of the higher lateral modes such as the 5th and 6th modes were slightly decreased, but these decreases are not very significant (1–3%).
- (2) The average damping ratios for higher vertical bending modes (3rd, 4th and 5th modes) are found within the range of 2–3% and show no significant changes with increased earthquake amplitude. The damping ratios for the last two torsional modes (2nd and 3rd modes) are

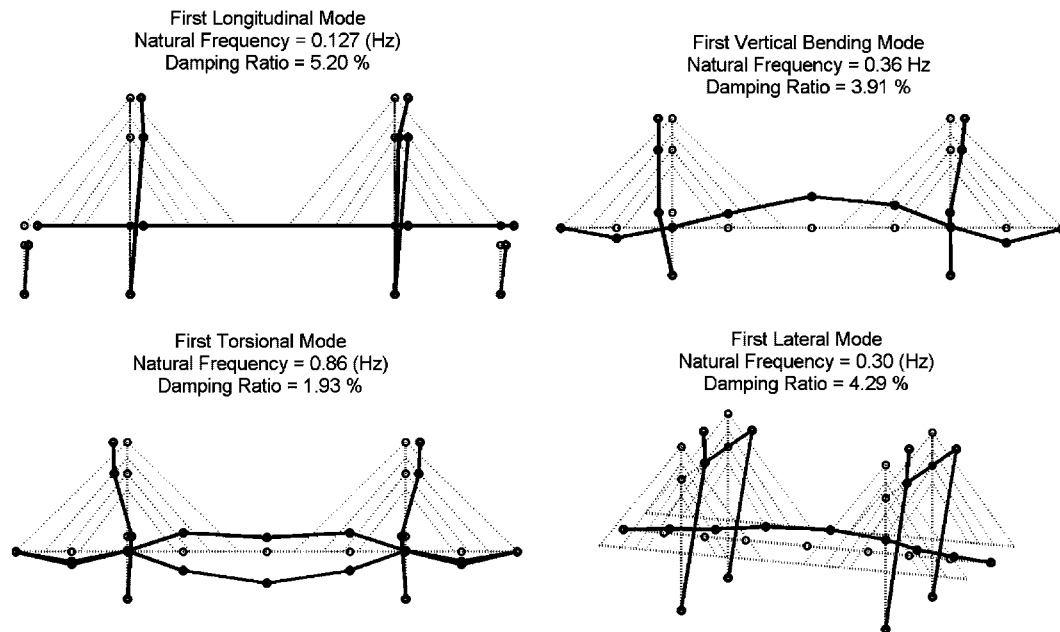


Figure 3. Representative shapes of the identified modes.

Table III. Set of input–output data from six earthquakes used in analysis.

No.	Earthquake (Frame number)	Maximum input acceleration ( $\text{cm/s}^2$ )	Data framing (s)	Data length (s)
1	20 February 1990 (3)	2.13	135.51–195.50	60
2	21 December 1996 (2)	2.45	58.61–113.50	55
3	5 June 1990	2.71	25.51–85.50	60
4	2 February 1992 (2)	4.16	65.51–125.50	60
5	21 December 1996 (1)	5.38	3.51–58.50	55
6	3 July 1995	5.62	20.01–80.00	60
7	20 February 1990 (2)	7.09	75.51–135.50	60
8	9 November 1996	7.88	30.01–90.00	60
9	20 February 1990 (1)	12.04	15.51–75.50	60
10	2 February 1992 (1)	13.08	5.51–65.50	60

also found in the range of 2–3% and mostly remain constant with increased earthquake amplitude. Average damping ratios for lateral modes, however, are higher than those of the vertical modes, with the range of average values 3–5%.

- (3) Damping ratios for lower modes (1st and 2nd modes) in both vertical and lateral direction show an increasing trend with the increase of earthquake magnitude. For small magnitude, average damping ratios are found to be 2% and increase significantly up to 4–5% as the earthquake magnitude increases. The largest damping ratios are found during the biggest

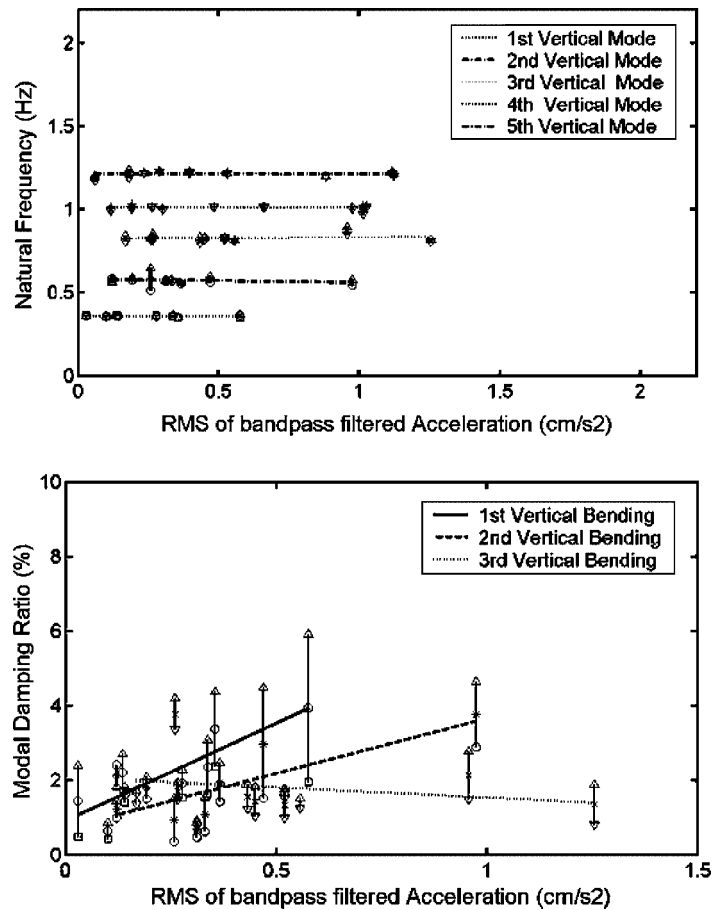


Figure 4. Variation of natural frequencies and damping ratios for vertical mode with respect to earthquake input amplitude.

earthquake (earthquake No. 10). This result indicates that damping for lower modes are dependent on earthquake amplitude, which might be due to the results of greater energy dissipation caused by friction in bearings that occurs during large earthquake.

In general, natural frequencies observed from earthquake records are identified within good agreement with the results from the ambient and forced vibration tests. Observation of the results shows that their values remain almost constant with respect to earthquake amplitude. Modal damping ratios, on the other hand, indicate a magnitude dependency, especially for several lower modes. Most damping ratios are identified with average values in the range of 0.5–5.5%. This lowest average value (0.5%) is satisfactory according to the minimum damping ratio required by the bridge seismic design and specification. The highest average value (5%), however, is much larger than the previously estimated (2%) from the study conducted by the Honshu-Shikoku Bridge Authority.

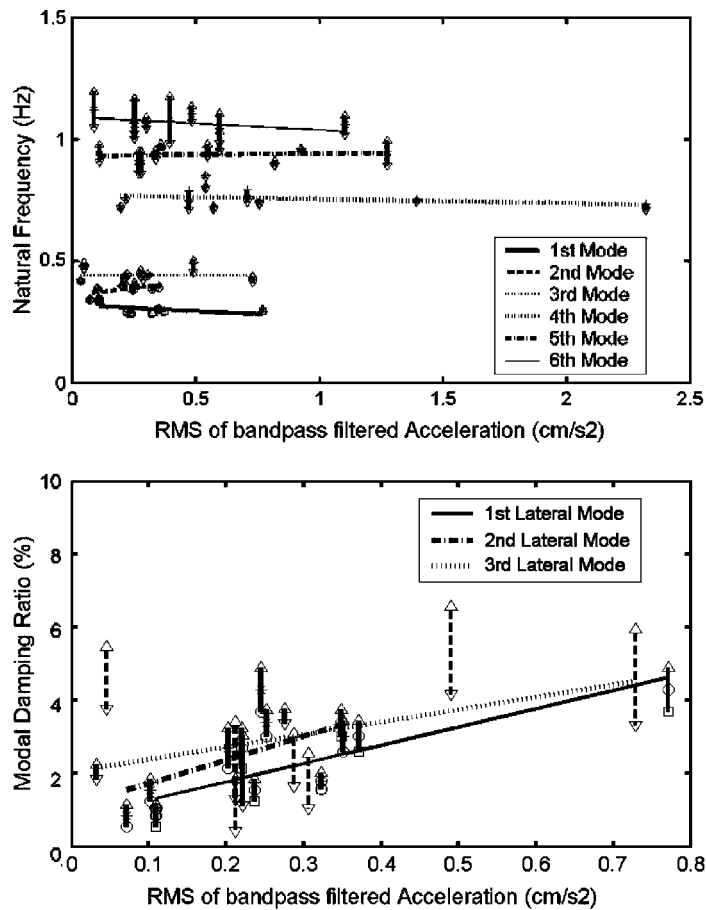


Figure 5. Variation of natural frequencies and damping ratios for lateral mode with respect to earthquake input amplitude.

### 6.2. Performance evaluation of link-bearing connection (LBC)

To enhance earthquake resistance, the effect of inertia force from the superstructure to substructure is limited by connecting the girder to towers and end-piers using a Link-Bearing Connection (LBC) [20, 21]. During earthquakes the LBC is designed to function as a perfectly hinged connection along the longitudinal axis. This implies that the girder and pier cap act as separated units and therefore the force from superstructure will not be transmitted to the piers. In designing the end-piers, this assumption of perfectly hinged connection was employed.

The actual performance of the LBC is studied by observing modal parameters of the first longitudinal mode identified from earthquake records. It should be noted that the longitudinal girder motion induces the non-linear behaviour of the link-bearing connections. This type of motion is excited only by earthquakes and is not measurable during ambient motion measurement and dynamic testing using exciters. Investigation of the LBC is performed by observing the relative modal displacement between pier cap and girder at both end-piers. This

relative modal displacement is quantified using a normalized relative modal displacement index ( $\phi$ ) defined as

$$\phi = \phi_{\text{girder}} - \phi_{\text{pier-cap}} \quad (22)$$

where  $\phi$  denotes the modal displacement with the maximum value normalized to unity. When the pier-cap and girder are largely separated as expected in the fully hinged mechanism, the index value is closer to unity; otherwise its value is close to zero. The results of system identification from 10 frames of earthquake are listed in Table IV. Figure 6 shows that there

Table IV. Modal parameters of the first longitudinal mode identified from six earthquakes.

No.	Earthquake (Frame number)	Maximum input acceleration (cm/s <sup>2</sup> )	Identified Freq (Hz)	Damp ratio (%)	Pier–Girder relative modal displ. ( $\phi$ )	
					Left-end pier	Right-end pier
1	20 February 1990 (3)	2.13	0.209	4.775	0.41	0.69
2	21 December 1996 (2)	2.45	0.213	5.255	0.55	0.67
3	5 June 1990 (1)	2.71	0.202	6.334	-0.25	-0.31
4	2 February 1992 (2)	4.16	0.223	2.751	0.20	-0.46
5	21 December 1996 (1)	5.38	0.216	9.214	0.24	-0.82
6	3 July 1995 (1)	5.62	0.221	3.614	0.79	-0.12
7	20 February 1990 (2)	7.09	0.129	11.630	0.20	-1.02
8	9 November 1996 (1)	7.88	0.234	6.215	-0.11	0.36
9	20 February 1990 (1)	12.04	0.128	5.203	0.72	0.60
10	2 February 1992 (1)	13.08	0.133	4.307	0.80	1.18

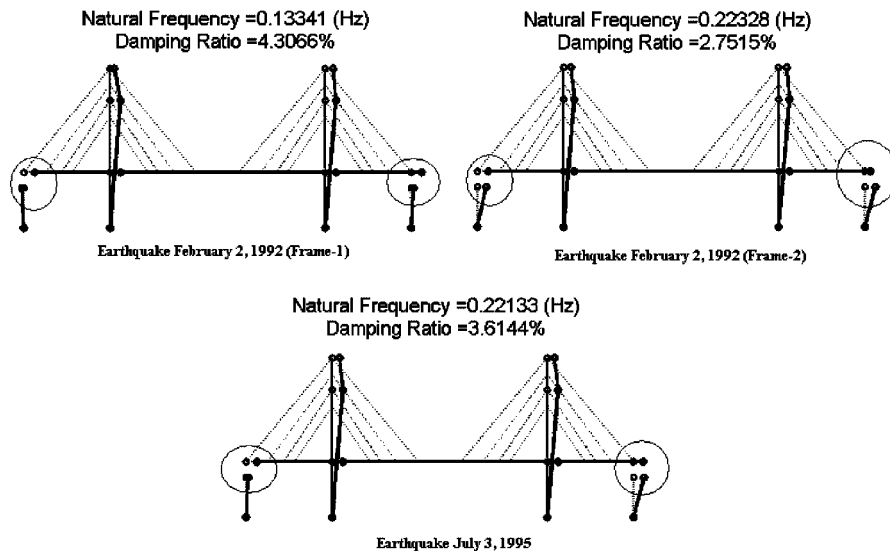


Figure 6. Three typical first longitudinal modes identified from system identification: (a) hinged-hinged mode; (b) fixed-fixed mode; and (c) hinged-fixed mode.

are three typical first longitudinal modes observed. The first mode was identified at around 0.128–1.334 Hz, which is a typical first mode with the hinged–hinged assumption of end-piers as predicted from the finite element model [20]. This mode shows a large relative modal displacement between the end-piers cap and the girder. The large gap here suggests that during the earthquake, the fully hinged mechanism at the connection between pier-cap and girder has taken place. The second and third modes were identified at higher frequencies between 0.18 and 0.24 Hz. The second mode displays a mixed mechanism in which by judging from the small relative modal displacement, one of the end-pier cap remains fixed or closely connected with the girder, while the other has developed the fully hinged mechanism. In the third mode, an even smaller relative modal displacement between pier cap and girder was observed at both end-piers. In this mode, both end-piers cap remain fixed or closely connected to the girder. The last two columns in Table IV list the index of relative modal displacement between pier-caps and girder of the left-end and right-end pier, respectively. The values of this index determine the condition of end-pier to girder connection and, thus, the type of identified mode as either hinged or fixed.

To have a better understanding of the hinged–hinged or fixed–fixed mechanism, displacement responses were analysed. For this purpose displacement responses were generated by double integration of the recorded accelerations after passing them through a band pass filter, which cut frequencies below 0.05 Hz and above 25 Hz. An example of displacement response from the earthquake on 2 February 1992 (earthquake #10) is presented in Figure 7. It can be observed

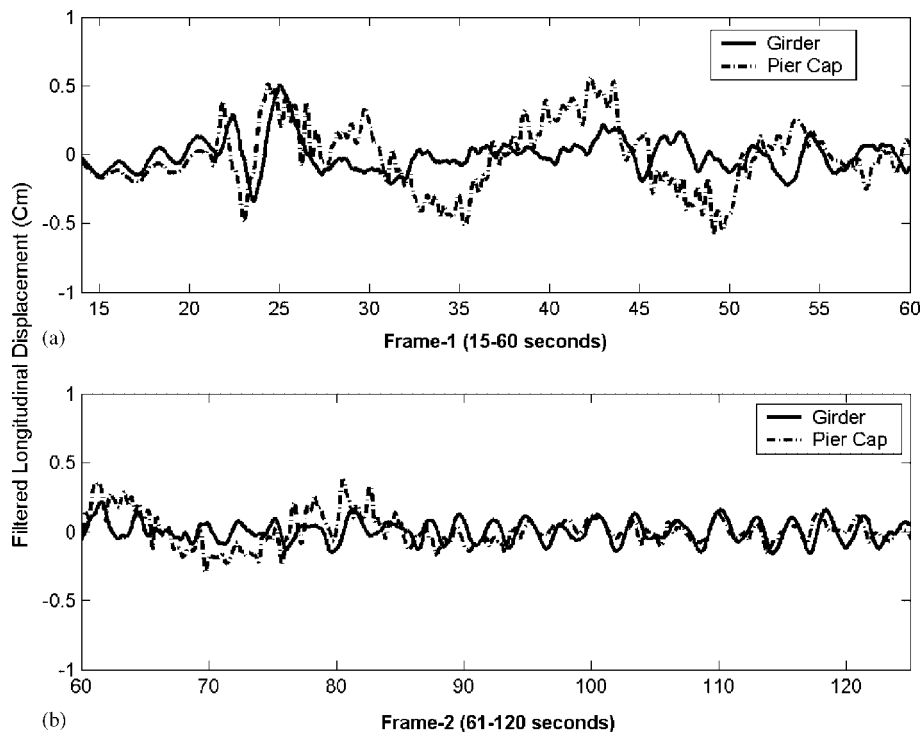


Figure 7. Filtered displacement response of the left-end pier cap from 2 February 1992 earthquake during: (a) hinged–hinged mode; and (b) fixed–fixed mode.

from this figure that displacement responses have two characteristics: (1) large gap between pier cap and girder during the peak of the earthquake (20–60 s), and (2) small insignificant relative displacement between pier cap and girder afterwards. During the last 60 s, displacement response becomes smaller and the discrepancy between the girder and pier-cap displacement becomes significantly reduced. System identification indicates two modes from this record, the hinged–hinged mode at 0.134 Hz for the first frame (time: 1–60 s), when the large gap is observed, and the fixed–fixed mode at frequency of 0.223 Hz for the second frame (time: 61–120 s). The index of relative modal displacement confirms the response analysis. For the first frame, the value of  $\varphi$  is 0.8 for the left-end pier and 1.18 for the right-end pier. For the second frame, the value of  $\varphi$  is 0.20 for the left-end pier and  $-0.46$  for the right-end pier.

Based on the system identification and analysis of response of Yokohama-Bay Bridge subjected to six earthquakes, it was observed that during small earthquakes the link-bearing connection has yet to function as a full-hinged connection. Therefore, a stiffer connection with higher natural frequency was observed. The mixed hinge-fixed mode was observed during smaller and moderate earthquake, which might be due to the variations of excitation level at the bottom of each pier. The full-hinged type of connection at both end-piers was only observed during the large earthquake. This hinged–hinged mode suggests that the link-bearings have performed as intended. The investigation performed here shows that during earthquakes, link-bearing connections might not perform as predicted or as modelled in finite-element. This deviation mechanism would have not been discovered without the vibration based system identification.

## 7. CONCLUSIONS

Dynamic performance of Yokohama-Bay Bridge is investigated by observing the trends of modal parameters identified from system identification. For system identification the realization method based on the SRIM is employed. This methodology utilizes the set of ground motions and structural vibration responses as input–output data set. The application to the Yokohama-Bay Bridge, has successfully demonstrated the feasibility of the actual application of algorithm. The benefits of this method are: (1) it identifies modal characteristics, such as natural frequencies, modal damping ratios and mode shapes with efficient use of relatively short earthquake record, (2) it is a data driven algorithm, which requires no prior knowledge of structural information, and (3) it allows the identification for SIMO system as well as MIMO system, making it well-suited for application on large, complex structures with multiple-inputs and multiple-outputs.

Using the system identification procedure, this study shows that it is possible to capture the global behaviour of a bridge such as amplitude-dependency of modal parameters during an earthquake and at the same time investigate the performance of local components such as link-bearing connection. The investigation of link-bearing connection using seismic records is particularly important since this type of motion is only observed during earthquakes and is not measurable during ambient motion measurement and dynamic testing using exciters. Long-term and dense-array seismic monitoring of Yokohama-Bay Bridges made it possible to capture this type of motion and to understand the actual seismic performance of link-bearing connection. The advantage of a long-term dense-array monitoring along with the efficient identification

scheme might lead to a promising future application for structural assessment and monitoring during seismic loading.

#### ACKNOWLEDGEMENTS

The authors gratefully acknowledge Tokyo Metropolitan Expressway Public Corporation for providing the strong motion records and construction drawing of the Yokohama-Bay Bridge. Valuable comments and data from Dr Masaaki Yabe of Chodai Consulting are also highly appreciated. The first author is thankful to the Japanese Ministry of Education, Culture, Sports, Science and Technology, for providing financial support during the study and this research at the University of Tokyo.

#### REFERENCES

1. Beck JL, Jennings PC. Structural identification using linear model and earthquake records. *Earthquake Engineering and Structural Dynamics* 1980; **8**:145–160.
2. McVerry GM. Structural identification in the frequency domain from earthquake records. *Earthquake Engineering and Structural Dynamics* 1980; **8**:161–180.
3. Chaudhary MTA, Abe M, Fujino Y, Yoshida J. System identification of two base-isolated bridges using seismic records. *Journal of Structural Engineering* (ASCE) 2000; **126**(10):1181–1194.
4. Koh CG, See LM. Identification and uncertainty estimation of structural parameters. *Journal of Engineering Mechanics* (ASCE) 1993; **120**(6):1219–1236.
5. Masry SF, Miller RK, Saud AF, Caughey TK. Identification of nonlinear vibrating structures. Part I: formulation. *Journal of Applied Mechanics* (ASME) 1987; **109**:918–922.
6. Masry SF, Miller RK, Saud AF, Caughey TK. Identification of nonlinear vibrating structures. Part II: application. *Journal of Applied Mechanics* (ASME) 1987; **109**:923–929.
7. Udawadia FE. Methodology for optimum sensor locations for parameter identification in dynamic system. *Journal of Engineering Mechanics* 1994; **120**(2):368–390.
8. Safak E. Adaptive modeling, identification and control of dynamic structural systems. I: theory. *Journal of Engineering Mechanics* 1995; **115**(11):2386–2405.
9. Safak E. Adaptive modeling, identification and control of dynamic structural systems. II: application. *Journal of Engineering Mechanics* 1989; **115**(11):2406–2426.
10. Beck JL, Katafygiotis S. Updating models and their uncertainties. I: Bayesian statistical framework. *Journal of Engineering Mechanics* 1998; **124**(4):455–461.
11. Beck JL, Katafygiotis S. Updating models and their uncertainties. II: model identifiability. *Journal of Engineering Mechanics* 1998; **124**(4):463–467.
12. Juang JN, Phan M, Horta LG, Longman RW. Identification of observer/Kalman filter Markov parameters: theory and experiments. *Journal of Guidance and Control Dynamics* 1993; **16**(2):320–329.
13. Juang JN, Pappa RS. An eigensystem realization algorithm for modal parameter identification and model reduction. *Journal of Guidance, Control, and Dynamics* 1985; **8**(5):620–627.
14. Juang JN, Cooper JE, Wright JR. An eigensystem realization algorithm using data correlations (ERA/DC) for modal parameter identification. *Control Theory and Advance Technology* 1988; **4**(1):5–14.
15. Juang JN. System realization using information matrix. *Journal of Guidance, Control, and Dynamics* 1997; **20**(3):492–500.
16. Smyth AW, Pei J-S, Masri SF. System identification of the Vincent Thomas Suspension Bridge using earthquake records. *Earthquake Engineering and Structural Dynamics* 2003; **32**(3):339–367.
17. Lus B, Betti R, Longman RW. Identification of linear structural system using earthquake-induced record. *Earthquake Engineering and Structural Dynamics* 1999; **28**:449–467.
18. Fujino Y, Kikkawa H, Namikawa K, Mizoguchi T. Seismic retrofit design of long-span bridges on metropolitan expressways in Tokyo. *Proceeding of the 6th International Bridge Engineering Conference, Transportation Research Board*, Boston, MA, U.S.A., 2005.
19. Siringoringo DM. System identification of bridges using seismic records and their performance evaluation. Doctoral Dissertation, Department of Civil Engineering, University of Tokyo, 2005.
20. *The Yokohama Bay Bridge*. The Metropolitan Expressway Public Corporation: Tokyo, Japan, 1991; 164–172 (in Japanese).
21. Maeda K, Otsuka A, Takano H. The design and construction of Yokohama Bay Bridge. In *Cable-Stayed Bridges Recent Developments and their Futures*, Ito M *et al.* (eds). Elsevier: Amsterdam, 1991; 377–395.